Chemical Science

ROYAL SOCIETY OF CHEMISTRY

EDGE ARTICLE

View Article Online
View Journal

Cite this: DOI: 10.1039/d6sc01678b

All publication charges for this article have been paid for by the Royal Society of Chemistry

Dual role of a conjugated bridge in intramolecular singlet fission: light-harvesting antenna and energy funnel

Jie Kong, [a] Kanad Majumder, [b] Manoj K. Sharma, [b] Soham Mukherjee, [c] Andrew J. Musser, [c] Satish Patil *[b] and Woojae Kim *[a]

Herein, an 'antenna-mediated' singlet fission (SF) molecular platform is reported, in which a phenyldiketopyrrolopyrrole (PDPP) chromophore with strong visible-light absorption is strategically integrated into TIPS-pentacene (P) dimers as a conjugated bridge to overcome the intrinsically weak absorption of conventional P-based SF systems. Owing to the complementary absorption and emission characteristics of PDPP and P, the resulting conjugates enable highly efficient intramolecular Förster resonance energy transfer (FRET) from PDPP to P, followed by intramolecular SF of the P dimer. Upon selective excitation of the PDPP antenna, ultrafast and nearly unity FRET occurs on a picosecond timescale, populating the singlet excited state of P and triggering SF with rates identical to those observed under direct P excitation. This demonstrates that antenna-mediated excitation fully preserves the intrinsic SF dynamics while extending excitation across the entire visible solar spectrum. The exceptional energy-transfer efficiency is rationalized by a large orientation factor, substantial spectral overlap, and the high fluorescence quantum yield of PDPP. Moreover, solvent polarity provides an external handle to modulate the spectral overlap and thereby tune both the FRET and SF rate constant, without requiring chemical modification of the molecular framework. Overall, this work establishes an antenna-enabled strategy for broadband solar-energy harvesting coupled to efficient SF, offering a general molecular design concept for next-generation SF materials with enhanced solar utilization efficiency.

Received 27th February 2026
Accepted 3rd June 2026

DOI: 10.1039/d6sc01678b

rsc.li/chemical-science

Introduction

Singlet fission (SF) has emerged as one of the most promising photophysical mechanisms to surpass the Shockley–Queisser (SQ) limit of single-junction solar cells. The SQ limit constrains the maximum power conversion efficiency of conventional single p–n junction devices to approximately 33%.[1] To overcome this fundamental restriction, extensive efforts have been devoted to multiexciton generation strategies, including carrier multiplication in inorganic semiconductors and SF in organic π-conjugated systems.[2–4] In SF, the excitation energy of an organic molecule promoted to its lowest singlet excited state (S_1) upon absorption of a single photon can be converted, in a spin-allowed manner, into a pair of triplet excitons (T_1) distributed over two neighboring chromophores. This process typically proceeds *via* the formation of a correlated triplet-pair (TT) intermediate, ^{m}(TT) (m = 1, 3, 5), which subsequently evolves into two spin-decorrelated free triplet excitons (T_1 + T_1).[5–8] Efficient SF requires stringent energetic and electronic coupling criteria, including $E(S_1) \sim 2E(T_1)$ to ensure thermodynamic feasibility and $E(T_2) > 2E(T_1)$ to suppress competing triplet–triplet annihilation pathways. In addition, suitably balanced electronic coupling between adjacent chromophores is essential for enabling SF dynamics, which can be achieved through crystal packing, high-concentration solutions, or covalently linked dimeric/oligomeric architectures.[8–12] Successful implementation of SF in photovoltaic devices is expected to raise the theoretical efficiency limit from ∼33% to approximately 44%,[13] motivating sustained interest in the molecular design, excited-state dynamics, and mechanistic understanding of SF materials over the past decade.[12,14–18]

To date, a wide variety of organic molecular systems have been reported to exhibit SF behavior, including acene derivatives,[19–23] 1,3-diphenylisobenzofuran and its derivatives,[24] rylene bisimides,[25–28] diketopyrrolopyrrole-based chromophores,[29] open-shell diradical compounds,[30,31] and carotenoid analogues.[32,33] Nevertheless, materials capable of ultrafast and efficient SF remain predominantly centered on pentacene-based chromophores. Owing to their strongly exothermic SF energetics ($E(S_1) - 2E(T_1) > 0.1$ eV) and well-resolved transient spectroscopic

[a]Department of Chemistry, Yonsei University, Seoul 03722, Republic of Korea. E-mail: woojae@yonsei.ac.kr

[b]Solid State and Structural Chemistry Unit, Indian Institute of Science, Bengaluru-560012, India. E-mail: spatil@iisc.ac.in

[c]Department of Chemistry and Chemical Biology, Cornell University, Ithaca, NY 14850, USA

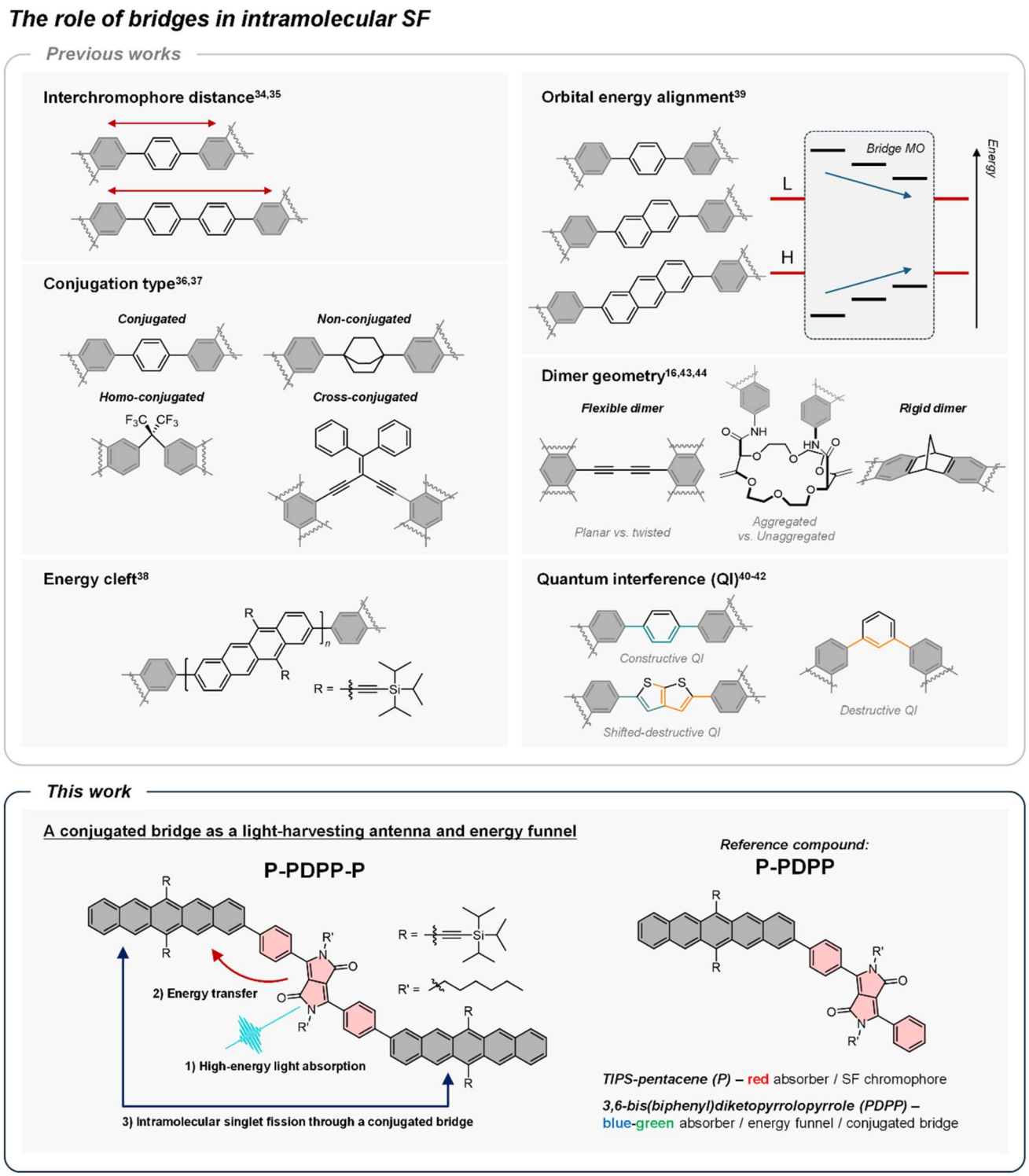

Fig. 1 Previously reported roles of bridges in P-based SF systems. The top side of the figure mainly presents an overview of the representative strategies for regulating SF rate through bridging design in previous studies, whereas the bottom side highlights the enhanced functionality of the bridge in this work. In this design, the PDPP bridge serves both as an efficient light-absorbing unit and as an energy funnel directing excitation toward the lower-energy P units. The bottom of the schematic shows the chemical structures of a PDPP-P conjugate (**P-PDPP-P**) investigated in this work, and a spectroscopic reference molecule **P-PDPP**.

signatures, pentacene derivatives have become benchmark systems for elucidating SF mechanisms and structure–property relationships. In this context, covalently linked pentacene dimers have proven to be particularly powerful model platforms, as they allow systematic control over interchromophoric coupling while avoiding the structural and morphological complexities inherent

to condensed-phase assemblies. Previous studies on pentacene dimers have largely focused on tuning electronic coupling through variations in bridge length,[34,35] conjugation topology (linear, cross-conjugated, homo-conjugated, or nonconjugated),[36,37] energy cleft formation,[38] orbital energy alignment,[39] quantum interference effects,[40–42] resonance effects,[39] and molecular geometry (Fig. 1),[16,43,44] with the primary goals of regulating SF rates and TT separation and of clarifying mechanistic pathways such as charge-transfer (CT)-mediated *versus* direct SF. Despite these advances, the practical application of P-based SF materials in photovoltaic devices remains limited by their relatively weak visible-light absorption, narrow absorption bandwidth, and insufficient photostability. For example, the widely studied 6,13-bis(triisopropylsilylethynyl)pentacene (TIPS-pentacene, P) exhibits a molar extinction coefficient (ε) of $\sim 2.1 \times 10^4$ M^{-1} cm^{-1} and absorbs predominantly around 640 nm, leaving a substantial portion of the visible solar spectrum underutilized.[34] Importantly, this limitation is not unique to P derivatives but is characteristic of many prototypical SF chromophores. Other widely investigated SF-active systems, such as tetracene derivatives and perylene bisimide based systems, similarly display relatively narrow absorption windows.[25,45] Consequently, developing SF-active molecular systems that combine efficient SF dynamics with broad and strong light absorption represents one of the critical challenges in the field.[46,47]

Herein, we showcase new facets of the role of a conjugated bridge in intramolecular SF in a molecular dimer. Rather than serving solely as a structural linker that modulates electronic coupling between P units and their conformations mentioned above, the bridge is deliberately designed to function as an active light-harvesting antenna, compensating for the intrinsic absorption range of P and efficiently funneling the harvested excitation energy into the SF-active chromophores.[48,49] This role is analogous to that of light-harvesting complexes in photosystems, which transfer absorbed energy to a reaction center for subsequent electron transfer.[50] While energy transfer from an isolated chromophore to a P dimer connected by non-conjugated chemical bonds has been reported, implementation of this concept through a conjugated bridge has remained unexplored.[48,51–54] Previous systems have established that an external sensitizer can broaden the excitation window of pentacene dimers and initiate SF through efficient intramolecular energy transfer.[48,51–54] In particular, Gotfredsen *et al.*[52] demonstrated that the relative spatial arrangement and transition dipole orientation between the sensitizer (subphthalocyanine) and the P dimer strongly affects the energy-transfer rate: the peripheral arrangement exhibits *ca.* 26-fold faster energy transfer than the axial analogue despite a longer donor–acceptor distance, owing to a much more favorable transition-dipole orientation and larger orientation factor. The finding highlights that antenna identity and spatial arrangement, rather than donor–acceptor distance alone, are decisive parameters for sensitized SF. Building on this mechanistic framework, the present work asks whether the bridge itself can be transformed from a passive structural linker into an active conjugated antenna that simultaneously broadens light absorption, enforces favorable dipole alignment, and preserves the intrinsic SF dynamics of the pentacene dimer. Specifically, we carefully select 3,6-bis(biphenyl) diketopyrrolopyrrole (PDPP) as the bridging chromophore owing to its intense absorption in the 400–550 nm region, which compared to subphthalocyanine-based systems, provides significantly enhanced light-harvesting capability in the 400–500 nm range,[52,55,56] high fluorescence quantum yield (~90%), and well-known sensitivity of its optical properties to adjacent aromatic substitution. Previous studies on SF molecules in which PDPP was introduced at the 6,6′-position of pentacene *via* ethynyl linkages successfully elucidated the role of dynamic structural fluctuations in governing SF dynamics.[56,57] However, in those architectures, direct attachment of PDPP to the ethynyl unit does not enhance its absorption in the 400–550 nm region, limiting its antenna function. To overcome this limitation, PDPP was introduced at the 2- and 2′-positions of P (Fig. 1), leading to the design of two new molecular architectures: **P-PDPP**, a P monomer, and **P-PDPP-P**, a P dimer whose combined absorption spans nearly the entire visible region of the solar spectrum. Remarkably, in the dimeric architecture, the light-harvesting capability associated with the PDPP segment is effectively amplified by a factor of three without increasing the number of PDPP units, highlighting 2,2′-position functionalization provides an effective means to magnify the absorption strength of PDPP through cooperative interactions with P units. Importantly, the PDPP unit retains its intrinsic electronic characteristics upon incorporation into the P framework, thereby preserving its electronic complementarity with P. The strong spectral overlap between PDPP emission and P absorption enables highly efficient, directional energy transfer from PDPP to P. Photophysical investigations, especially transient absorption (TA) experiments, reveal that selective excitation of PDPP in **P-PDPP-P** leads to SF dynamics that are indistinguishable from those observed upon direct excitation of P, indicating near-unity energy-transfer efficiency mediated by ultrafast Förster resonance energy transfer (FRET). This 'antenna-mediated' SF process demonstrates a viable strategy for achieving broadband solar harvesting while maintaining the intrinsic SF performance of P, thereby offering new design principles for next-generation SF materials with enhanced solar utilization.

Results and discussion

Synthesis

The targeted molecules **P-PDPP** and **P-PDPP-P** were synthesized *via* a carbon–carbon Suzuki–Miyaura coupling reaction between the respective di/mono-iodo derivative of diketopyrrolopyrrole (the bridge moieties) and the borylated pentacene precursor in the presence of palladium catalyst $Pd(dppf)_2Cl_2 \cdot DCM$ and K_2CO_3 in a tetrahydrofuran (THF), water (10 : 1) mixture. The synthetic route and the molecular structures are illustrated in Scheme S1. Targeted compounds were purified by silica gel chromatography; structures and purity were confirmed by ^1H, ^{13}C and MALDI-TOF (Fig. S1–S8).

Steady-state optical properties

To evaluate the capability of PDPP to function as a visible-light-harvesting antenna and a directional energy-transfer donor for P-centered intramolecular SF, steady-state optical properties

were collected for **P-PDPP**, **P-PDPP-P**, and the reference compounds P and PDPP in solvents of varying polarity (Fig. 2, S9 and S10). From the absorption spectra in Fig. 2A, a preliminary assessment can be made regarding the ground-state interactions between the two P units and between pentacene and the PDPP core in **P-PDPP-P** and **P-PDPP**. Both **P-PDPP** and **P-PDPP-P** in THF exhibit two well-defined absorption manifolds: a lower-energy band spanning 550–700 nm, exhibiting the well-resolved vibronic structure characteristic of P units, and a higher-energy band between 400 and 550 nm arising predominantly from the PDPP unit. These spectra can be approximated as a linear combination of the monomeric P and PDPP spectra, indicating that PDPP effectively complements the missing visible-region absorption of P and thus substantially broadens the effective optical coverage across the visible spectrum. Closer inspection, however, reveals subtle deviations.

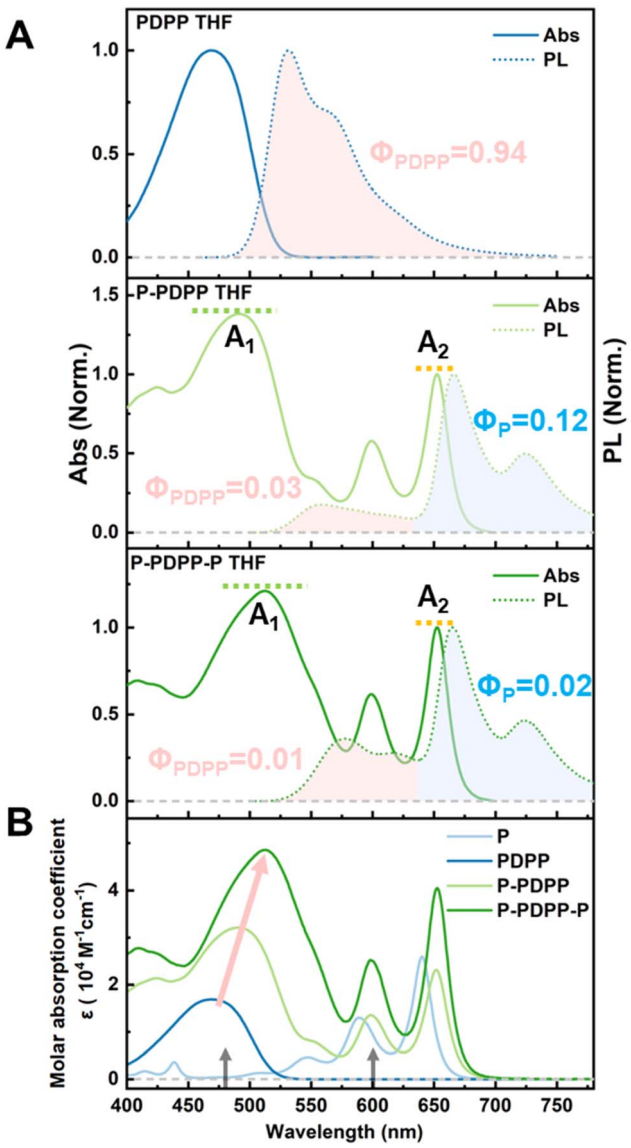

Fig. 2 Steady-state absorption and photoluminescence (λ_{exc} = 400 nm) spectra of (A) PDPP, **P-PDPP** and **P-PDPP-P** in THF. (B) Molar absorption coefficients spectra of P, PDPP, **P-PDPP** and **P-PDPP-P** in THF. The black arrows denote excitation energies used in the TA experiments.

In **P-PDPP**, the pentacene $S_0 \rightarrow S_1$ transition is red-shifted by approximately 36 meV relative to the P reference, and the PDPP-associated absorption band exhibits a red shift of ~113 meV relative to the PDPP reference. These shifts indicate that pentacene and PDPP exhibit a degree of ground-state electronic interaction in **P-PDPP**. Upon introduction of a second P unit, the P-derived absorption maxima in **P-PDPP-P** remain essentially unchanged relative to those in **P-PDPP**, demonstrating negligible direct electronic coupling between the two P units. The conclusion is further supported by density functional theory (DFT) calculations, as shown below, which show a large interunit separation of about 26.6 Å. In contrast, the PDPP-centered absorption band continues to red-shift by ~113 meV upon going from **P-PDPP** to **P-PDPP-P**, suggesting that increasing the number of P units enhances the electronic interaction between PDPP and its neighboring P moieties, though not to an extent sufficient to produce a new distinct CT band in the ground state. Moreover, an intriguing trend emerges from the relative intensities of the PDPP-dominated (A_1) and pentacene-dominated (A_2) absorption bands: in both **P-PDPP** and **P-PDPP-P**, A_1/A_2 remains essentially constant (*e.g.*, ~1.2 in THF). Given that **P-PDPP-P** contains twice the number of pentacene chromophores, one would anticipate a twofold decrease in A_1/A_2 compared with **P-PDPP**. To clarify this inconsistency, we compared the molar absorption coefficients ε (Table S1) of those molecules. The ε of the pentacene unit in **P-PDPP** closely matches that of P, whereas in **P-PDPP-P** it increases to ~1.7× that of **P-PDPP**, which is fully reasonable given the additional pentacene unit. Surprisingly, the ε of the PDPP core also increases as the number of P units grows (from $1.69 \times 10^4 \rightarrow 3.21 \times 10^4 \rightarrow 4.86 \times 10^4$ M^{-1} cm^{-1}), even though the number of PDPP chromophores remains constant. This unexpected cooperative enhancement indicates that the light-harvesting ability of PDPP can be easily amplified by the connected P units, the origin of which will be further examined through quantum chemical analysis below. Finally, increasing the solvent polarity from hexane (HEX) to benzonitrile (BZN) (Fig. S9) induces only modest red shifts in the absorption spectra of both **P-PDPP** and **P-PDPP-P**, without altering the relative intensities of the A_1 and A_2 bands.

Steady-state photoluminescence (PL) measurements further elucidate the excited-state interactions between the PDPP core and the P units in **P-PDPP** and **P-PDPP-P**. Notably, when selectively exciting the PDPP unit (λ_{exc} = 400 nm), the resulting emission profiles of both compounds do not arise exclusively from the lowest singlet excited state (S_1), but instead display pronounced anti-Kasha-type high-energy emission. The PL spectra (Fig. 2A) can be decomposed into contributions from both the PDPP and P chromophores, indicating that—although weak ground-state interactions are present—the two units largely retain their independent absorption and PL characteristics in both **P-PDPP** and **P-PDPP-P**. This conclusion is supported by PL excitation spectra (Fig. S11): when monitoring PL at 720 nm, the excitation spectrum nearly mirrors the corresponding absorption spectrum. This behavior indicates that

measurable P emission is observed even upon selective excitation of the PDPP segment, suggesting the existence of an energy transfer process from PDPP → P. In addition, the optical bandgap trends derived from the PL spectra are consistent with those obtained from electrochemical measurements (Fig. S12), and the energy level distribution of the PDPP core effectively spans and overlaps the bandgap range of P units. Given the substantial spectral overlap between PDPP PL and P absorption, FRET is likely responsible for this process. In later sections, ultrafast transient spectroscopic measurements, combined with theoretical analysis of energy transfer, are used to rule out the possibility of Dexter-type electron-exchange energy transfer. In addition, the emission of **P-PDPP-P** exhibits a pronounced red shift with increasing solvent polarity: the PL 0–0 peak moves from 650 nm (1.91 eV) in HEX to 683 nm (1.81 eV) in BZN. Given that the triplet energy of P is *ca.* 0.86 eV (≈1440 nm),[58] the combined energy of two pentacene triplets is approximately 1.72 eV. This trend indicates a slight decrease in the S_1 energy of **P-PDPP-P** with increasing solvent polarity, thereby enabling modulation of SF energetics.

PL quantum yields and lifetimes provide quantitative insight into the hierarchy of excited-state deactivation pathways in these chromophores. The PDPP reference exhibits a very high fluorescence quantum yield ($\Phi_{PL} = 0.85$–0.97, Table S2), whereas the residual PDPP emission in both **P-PDPP** and **P-PDPP-P** is almost completely quenched ($\Phi_{PL} < 0.05$). Such a near-total quenching indicates that excitation of the PDPP unit is funneled with near-unity efficiency into the P units. Nevertheless, the highly weak residual PL signal is attributed to a minor sub-ensemble in which energy transfer does not occur, and PDPP acts as an independent emitter. This PL signal provides additional insight into the major sub-ensemble in which energy transfer occurs. As the solvent polarity increases, the PDPP-associated emission in **P-PDPP** and **P-PDPP-P** undergoes a progressive red-shift, which could enhance the spectral overlap between PDPP emission and P absorption, thereby possibly promoting PDPP → P FRET. Importantly, this behavior is similar in both **P-PDPP** and **P-PDPP-P**, however, the subsequent fate of the P excited state differs fundamentally between the two architectures. In **P-PDPP-P**, P-centered PL is almost suppressed in all solvents, indicating the opening of an additional ultrafast and highly efficient nonradiative decay channel. In **P-PDPP**, relative to the P monomer ($\Phi_{PL} \sim 0.36$ in THF),[59] the PL quantum yield of the P unit in **P-PDPP** is also significantly reduced ($\Phi_{PL,P} \sim 0.11$ in THF), indicating that PDPP modulates the excited-state dynamics of the P moiety. PL lifetime measurements (Table S2 and Fig. S13) are fully consistent with this picture. The PDPP exhibits solvent-independent lifetimes consistent with its solvent-insensitive quantum yield, whereas the lifetimes of the P units in **P-PDPP** (∼4.9 ns in THF) are substantially shorter than that of the P monomer (∼14 ns in THF),[59] confirming the emergence of accelerated nonradiative decay channels upon incorporation of the PDPP unit. Together, the quantum yield and lifetime data establish a clear mechanistic sequence in which PDPP-mediated energy harvesting is followed by the relaxation pathways of the excited state depend strongly on the number of P units, with SF uniquely enabled in the **P-PDPP-P** architecture.

Quantum chemical analysis

To elucidate the origin of the enhanced ε associated with the PDPP unit upon P incorporation, a detailed quantum-chemical analysis was carried out using DFT. Geometry optimization reveals that the two P units in **P-PDPP-P** adopt an almost orthogonal arrangement, with a dihedral angle of approximately 80° and a center-to-center separation of about 26.6 Å (Fig. S14). This geometry is consistent with the very weak ground-state electronic coupling inferred from steady-state spectroscopy, a feature commonly observed in 2,2′-linked P dimers. To more rigorously determine whether the weak electronic coupling between the P units arises from their relative orientation (with dihedral angles approaching either perpendicular or parallel) or from their large spatial separation, the mutual orientation of the P moieties was varied and three additional optimized geometries were obtained. By analyzing the frontier molecular orbitals (Fig. S15), vertical excitation energies (Table S3), and electron density difference plots (Fig. S16) for all four conformations, it was found that in the **P-PDPP-P** system the dominant factor governing the absorption properties and mutual interactions of the P units is their spatial separation rather than their relative dihedral angle. In contrast, as the number of appended P units increases from PDPP to **P-PDPP** and further to **P-PDPP-P**, the dihedral angles between the diketopyrrolopyrrole core of PDPP and the adjacent phenyl rings systematically decrease (Table S4), rendering the PDPP backbone progressively more planar. The increased planarity effectively extends π-conjugation within the PDPP segment and enhances electronic delocalization, narrowing the HOMO–LUMO energy gap (Table S5 and Fig. S17), which accounts for the experimentally observed red shift of the PDPP-associated absorption band.

Time-dependent DFT (TD-DFT) calculations were subsequently performed to simulate the absorption spectra, and the computed results are in excellent agreement with experiment (Fig. 3A). In **P-PDPP**, the lowest-energy transition appears at nearly the same wavelength as that of the P reference, with only a slight red-shift and an oscillator strength comparable to the monomer P unit. In **P-PDPP-P**, the two P units are separated by a large distance and largely retain their localized electronic character, rendering the HOMO/HOMO−1 and LUMO/LUMO+1 pairs quasi-degenerate in energy. As a result, the $S_0 \rightarrow S_1$ (612 nm) and $S_0 \rightarrow S_2$ (611 nm) transitions lie extremely close in energy and together constitute the lowest-energy absorption band. This near-degeneracy effectively doubles the total oscillator strength associated with the P-derived absorption, leading to a simulated ε of the P-band approximately twice that of **P-PDPP**, in excellent agreement with the experimental trend.

The pronounced enhancement of the PDPP-centered absorption was further examined by electron–hole density analysis, which reveals the nature of the higher-energy electronic transitions dominated by π–π* excitation of the PDPP backbone. With increasing numbers of appended P units, the

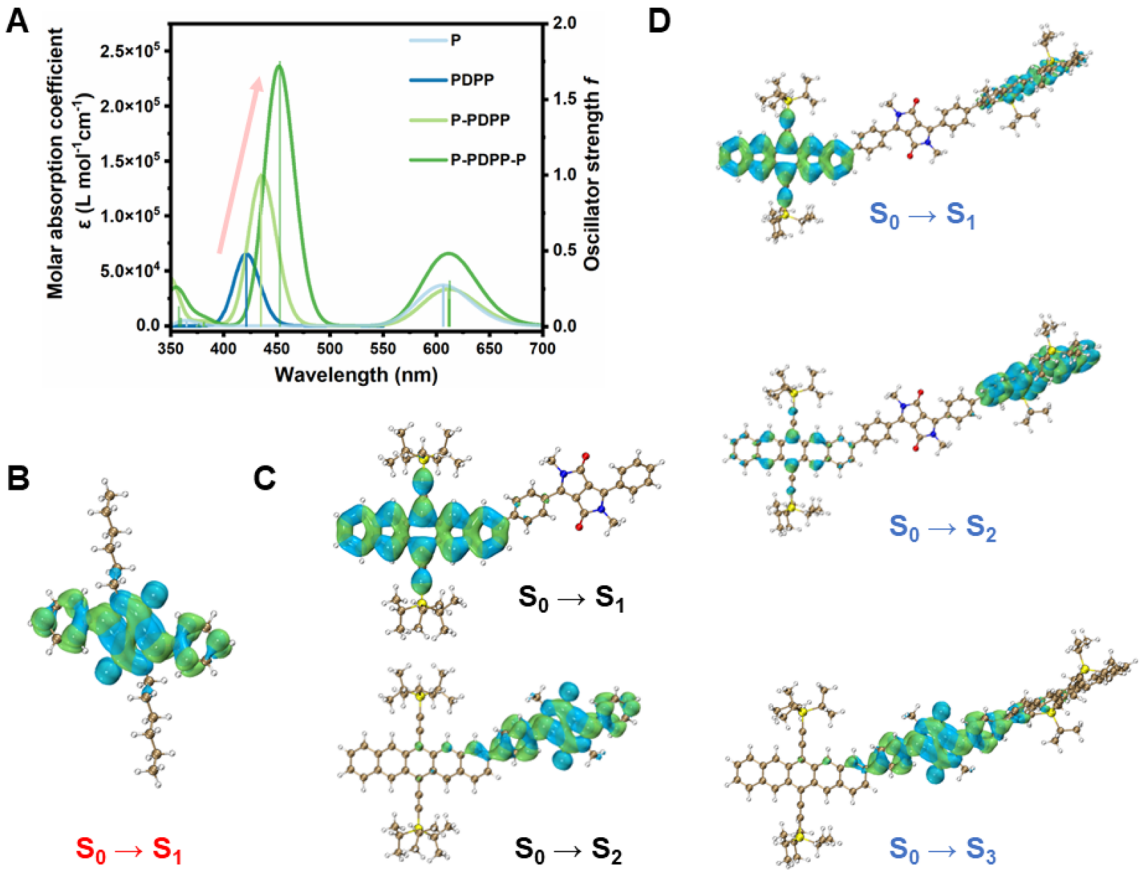

Fig. 3 (A) Simulated absorption spectra based on the results of TD-DFT. The excited state electron–hole analysis of (B) PDPP, (C) **P-PDPP**, and (D) **P-PDPP-P**. The isovalue is set as 0.0004. The green and blue denote the electron and hole, respectively.

PDPP-associated absorption band exhibits a substantial increase in oscillator strength, transition dipole moment, and calculated molar extinction coefficient, accompanied by a progressive red shift (Table S6). The charge density difference (CDD) map[60,61] reveals that for the ~450 nm transitions in both **P-PDPP** and **P-PDPP-P** (Fig. 3B and C), the hole–electron density is no longer strictly confined to the PDPP core (Fig. 3A) but becomes partially delocalized toward the appended P units. This trend is corroborated by transition orbital composition analysis (Table S6). In **P-PDPP-P**, the PDPP-dominated high-energy transition comprises multiple orbital contributions, including H−2 → L+2 (59.4%), H−2 → L (20.0%), and H → L+2 (10.8%), indicating that the ~450 nm absorption band is not a purely localized π–π* excitation within PDPP but instead contains a non-negligible CT component from the PDPP core toward the P fragments. The increasing CT character leads to a pronounced enhancement of the transition dipole moment, which increases systematically from PDPP (μ = 6.71 D) to **P-PDPP** (μ = 14.52 D) and further to **P-PDPP-P** (μ = 26.07 D). Consequently, the molar absorption coefficient associated with the PDPP-centered transition grows substantially as the number of appended P units increases. To further demonstrate the facile tunability of the PDPP absorption strength, model systems bearing one or two phenyl substituents appended to the PDPP core were constructed and analyzed (Fig. S18 and Table S7). Introduction of a single phenyl ring induces a red shift of the $S_0 \rightarrow S_1$ transition from 2.943 eV to 2.89 eV, accompanied by an increase in oscillator strength from 0.484 to 0.604. Additional phenyl substitution further enhances both the red shift and oscillator strength. The results highlight a key advantage of PDPP as a light-harvesting unit in SF architectures: its absorption can be readily amplified through conjugative coupling with appended P units, without the need for elaborate structural modification of the PDPP core itself.

Ultrafast energy transfer dynamics in P-PDPP

Femtosecond and nanosecond TA (fs-TA and ns-TA) measurements were performed to elucidate the energy transfer dynamics within **P-PDPP**. Excitation at 480 nm and 600 nm was employed to selectively populate the PDPP unit or the P units, respectively, enabling direct interrogation of the photoinduced relaxation pathways. In THF, fs-TA spectra recorded following 480 nm excitation are initially dominated by an excited-state absorption (ESA) feature at approximately 730 nm (ESA1), together with a ground-state bleach (GSB) at around 495 nm (Fig. 4A). The features coincide with the transient spectral signatures of the PDPP reference (Fig. S19) and are therefore assigned to the $S_1 \rightarrow S_n$ transition and GSB of the PDPP unit, confirming that 480 nm excitation selectively populates the

PDPP-associated S_3 state. ESA1 decays rapidly within a few picoseconds, concomitant with the emergence of new ESA bands at approximately 450 (ESA2) and 540 nm and a GSB near 650 nm (Fig. 4B), which closely match the characteristic fingerprints of the S_1 state of P. No signals attributable to radical ions of P are detected, ruling out photoinduced electron transfer from PDPP to P. The prompt appearance of P-like excited-state features following decay of the PDPP-localized excitation demonstrates efficient intramolecular energy transfer from PDPP to P.

Upon switching the pump wavelength to 600 nm (Fig. 4D), singlet excited-state features of P appear instantaneously, characterized by ESA at approximately 450 and 540 nm together with vibronically structured GSB at around 600 and 650 nm, while no PDPP-associated ESA signals are observed (Fig. 4E). Notably, both the GSB at 650 nm and the ESA2 at 450 nm reach their maximum intensities at time zero, confirming that 600 nm selectively excites only the P unit. Global analysis was performed on the fs-TA data of **P-PDPP** (Fig. 4C/F) to identify the short-lived intermediates and rate involved in the excited-state relaxation pathways. Under 480 nm excitation, a sequential kinetic model was employed. The first component (evolution associated difference spectra, EADS1; decay associated difference spectra, DADS1) is assigned to excitation localized on the PDPP unit, which rapidly transfers its energy to the P moiety with a time constant of 0.8 ps. In particular, the negative and positive amplitudes observed in the ESA regions of P and PDPP in DADS1, respectively, further corroborate the energy transfer dynamics. The subsequent component (EADS2, DADS2) is attributed to the excited state of P. In contrast, under 600 nm excitation, only EADS component associated with P is observed, consistent with the selective excitation of the P unit. Changing solvent polarity (Fig. S20–S22) does not alter the qualitative spectral evolution under either excitation wavelength; however, the energy-transfer kinetics accelerate systematically with increasing polarity, as revealed by global analysis of the fs-TA data (Table S10). This trend implies that solvation-induced relaxation increases the spectral overlap between the PDPP donor and the P acceptor units.[62,63]

The ultrafast energy-transfer process observed in **P-PDPP** can be rationalized by considering its underlying mechanism. Structural analysis indicates that the donor–acceptor center-to-center distance in **P-PDPP** is approximately 13.3 Å (Fig. S28), well beyond the distance required for efficient Dexter-type energy transfer.[64] In addition, the weak orbital overlap between the PDPP and P units could further suppress electron-exchange-mediated Dexter transfer. By contrast, FRET is fully compatible with these structural and spectral overlap conditions. According to the fundamental FRET rate expression (SI, S6 section), the transfer rate is dictated by the orientation factor (κ^2), the spectral-overlap integral (J), the donor emission quantum yield, and the refractive index of the medium (Table 1). Quantum calculations provide an orientation factor $\kappa^2 \approx 1.15$ for **P-PDPP**, derived from the relative orientations of the PDPP emission transition dipole and the P absorption transition dipole. This value is nearly twice the canonical $\kappa^2 \approx 0.67$ expected for flexible systems, indicating that the donor–acceptor geometry in **P-PDPP** is particularly favorable for

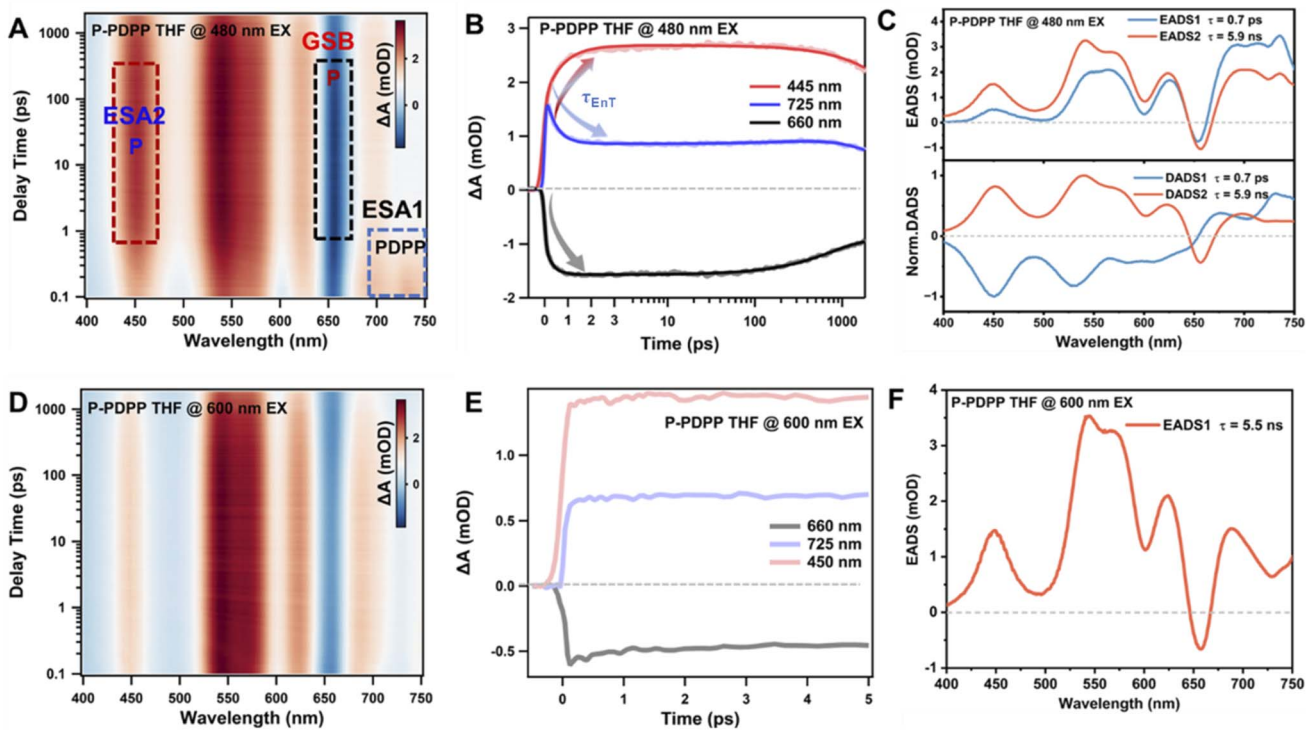

Fig. 4 fs-TA heat maps of **P-PDPP** in THF at 480/600 nm (A and D) excitation, selected single wavelength kinetics traces (B and E), and evolution/different associated difference spectra (C and F) obtained from a global analysis. In panel (B), EnT denotes energy transfer.

Table 1 Parameters used to calculate the intramolecular FRET rate constants of P-PDPP in different solvents

P-PDPP (R_{DA} = 1.33 nm)					
	n	J (spectral-overlap integral)	R_0 (nm)	k_{FRET} (s^{-1})	E
HEX	1.375	9.2461×10^{14}	5.30	7.205×10^{11}	0.9998
TOL	1.496	1.0055×10^{15}	5.12	5.619×10^{11}	0.9998
THF	1.407	9.5302×10^{14}	5.34	6.862×10^{11}	0.9997
BZN	1.528	1.0198×10^{15}	5.13	5.313×10^{11}	0.9997

efficient energy transfer.[52] Consistent with steady-state spectroscopy, increasing solvent polarity from HEX to THF to BZN systematically enhances the spectral overlap between PDPP emission and P absorption, thereby increasing J. The calculated FRET rates are on the order of 10^{11}–10^{12} s^{-1} and reproduce the experimental values with good agreement (*e.g.*, 6.86×10^{11} s^{-1} calculated *versus* 1.43×10^{12} s^{-1} measured in THF), validating FRET as the dominant transfer mechanism. Notably, the experimentally extracted rates are consistently somewhat larger than the purely dipole–dipole predictions. This systematic deviation suggests that, in addition to long-range Förster coupling, weak short-range interactions—such as through-bond electronic coupling or vibronic mixing between PDPP and P excited states—may provide an auxiliary channel that enhances the overall energy transfer rate. In this picture, energy transfer remains primarily Förster-type but is subtly accelerated by additional electronic communication within the covalently linked framework. The theoretical rates in BZN are underestimated due to limitations in the model's treatment of solvent refractive index. Because the Förster radius (R_0) substantially exceeds the donor–acceptor separation (R_{DA}), the overall transfer efficiency approaches unity, in excellent agreement with the ~100% efficiency extracted from TA measurements (Table S8).

It is instructive to compare these FRET parameters with those reported for previously developed subphthalocyanine–P systems. In the axial/peripheral subphthalocyanine–P conjugates reported by Gotfredsen *et al.*, both systems displayed near-unity energy-transfer efficiencies, but the peripheral arrangement exhibited substantially faster energy-transfer (0.3 ps^{-1} *vs.* 8.1 ps^{-1} for the axial geometry) because of its more favorable transition-dipole alignment, with κ^2 increasing from 0.08 in the axial geometry to 1.46 in the peripheral geometry.[52] Our PDPP-linked system follows the same design principle: despite its compact bridge-based architecture, **P-PDPP** possesses a large orientation factor of $\kappa^2 \approx 1.15$, comparable to the favorable peripheral configuration in the subphthalocyanine system. Accordingly, the calculated FRET rates of **P-PDPP** are in the 10^{11}–10^{12} s^{-1} range, and the experimentally extracted transfer rate in THF reaches 1.43×10^{12} s^{-1}, corresponding to sub-picosecond energy transfer and near-unity efficiency.

The longer-timescale excited-state evolution of **P-PDPP** was probed by ns-TA spectroscopy (Fig. S23–S26) to rationalize the reduced PL quantum yield of the P unit. Within the first ~20 ns, the transient spectra closely resemble the ~1 ns fs-TA spectra and are dominated by the S_1 features of P. At longer delay times, the signal amplitude decreases sharply and evolves into a spectrum characterized by a prominent ESA band at approximately 500 nm, identical to the triplet-state signature of P obtained from triplet sensitization experiments (Fig. S27). This evolution indicates that the long-time dynamics of **P-PDPP** are governed by intersystem crossing (ISC) from the P singlet state. Compared with the P reference (τ_{S1} = 14 ns, Φ_{PL} = 0.36 in THF),[59] the ISC process in **P-PDPP** is markedly accelerated, consistent with faster S_1 decay (τ_{S1} = 6 ns, THF) and the suppressed PLQY ($\Phi_{PL,P}$ = 0.11 in THF). The ns-TA spectra are independent of excitation wavelength and show no detectable PDPP-related features, demonstrating that the long-lived excited-state dynamics of **P-PDPP** are dominated entirely by P-derived states. Consistently, ns-TA measurements of the PDPP reference yield an excited-state lifetime of ~7 ns (Fig. S19), confirming that the PDPP excited state is efficiently quenched within the **P-PDPP** architecture.

Ultrafast energy transfer and intramolecular singlet fission in P-PDPP-P

To elucidate how the excited-state dynamics evolve upon incorporation of a second P unit, ultrafast spectroscopic measurements were performed on **P-PDPP-P** as well, under excitation conditions that selectively address either the PDPP or the P units. In THF, selective excitation of the PDPP unit at 480 nm initially produces a spectral evolution closely resembling that observed for **P-PDPP**, characterized by ultrafast FRET from PDPP to P within the first few picoseconds (Fig. 5A). This allows us to confirm that PDPP identically functions as an efficient light-harvesting antenna that rapidly funnels excitation energy into the P manifolds. For the **P-PDPP-P** system, the P acceptor possesses roughly twice the molar absorption coefficient compared to **P-PDPP**, leading to an approximately two-fold increase in J and therefore a faster FRET rate (1.56×10^{12} s^{-1}, Tables S8 and S9). This trend is consistent with the experimentally observed acceleration of PDPP → P energy transfer (0.5 ps, Table S10) in the dimeric architecture with respect to **P-PDPP**. The enhanced FRET rate observed in **P-PDPP-P** relative to **P-PDPP** may also arise from the increased number of energy-accepting units from the statistical point of view, as **P-PDPP-P** contains two P moieties whereas **P-PDPP** contains only one. Beyond this initial energy-transfer regime, however, the subsequent spectral evolution deviates markedly from that of **P-PDPP**. A weak ESA feature near 500 nm is already discernible within the first few hundred femtoseconds; however, its amplitude grows substantially on the tens-of-picoseconds timescale, accompanied by the renewed growth of a GSB near 650 nm. These features correspond to the formation of the spin-correlated triplet-pair state with overall singlet character, ^{1}(TT), which becomes fully established within approximately 100 ps (τ_{SF} ~ 20 ps), more than two orders of magnitude faster than the triplet formation observed for P in **P-PDPP** (~6 ns, Fig. S24). We found that increasing the solvent polarity slows the formation of ^{1}(TT) (Fig. S29–S31): the formation time increases from 13 ps in HEX to 33 ps in BZN (Table S10 and

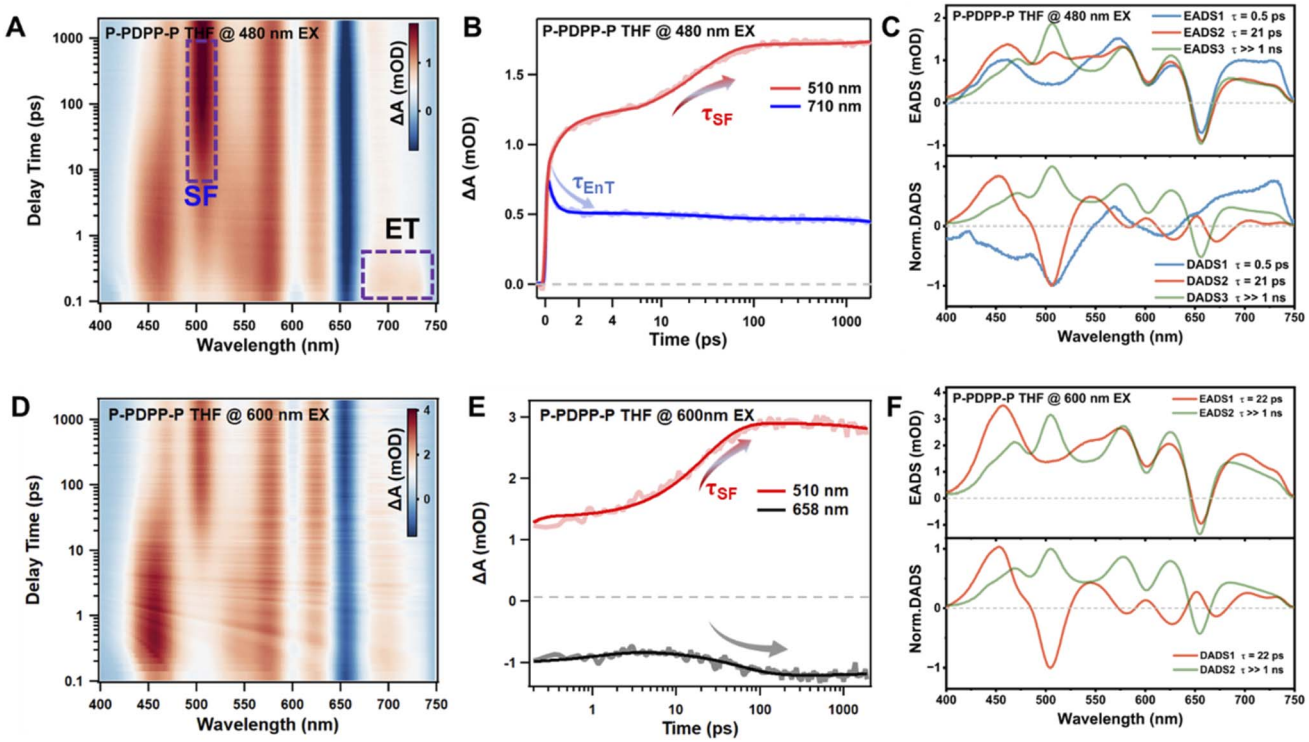

Fig. 5 fs-TA heat maps of **P-PDPP-P** in THF at 480/600 nm (A and D) excitation, selected single wavelength kinetics traces (B and E), and evolution/decay associated difference spectra (C and F) obtained from a global analysis. In panels (B and E), EnT and SF denote energy transfer and singlet fission, respectively.

Fig. S32). This trend can be attributed to a polarity-induced change in the relative energy alignment between S_1 and ^{1}(TT), which in turn reduces the driving force for SF and thereby decreases the rate. Closer inspection of the DADS obtained from global analysis provides additional mechanistic insight. In particular, DADS1 (Fig. 5C), corresponding to the sub-picosecond component assigned primarily to the decay of excited PDPP, exhibits an inverted spectral feature near 505 nm, coinciding with the characteristic ESA of ^{1}(TT) of a P dimer. Although the dominant pathway might remain sequential energy transfer followed by SF based on Kasha's rule, the presence of this subtle inverted signature suggests that some fraction of the initially excited PDPP population may couple directly into the ^{1}(TT) manifolds. This contribution might be small relative to the FRET-mediated channel but indicates that small but significant bridge-mediated electronic communication may facilitate direct population of ^{1}(TT) under selective PDPP excitation. To our knowledge, such direct initiation of SF from a chemically distinct donor chromophore into an acceptor dimer has not been previously reported. When the excitation wavelength is changed to selectively excite the P units directly at 600 nm, the fs-TA spectral evolution remains essentially identical to that observed under PDPP excitation, except for the absence of the initial PDPP-to-P energy transfer component (Fig. 5B and F). Furthermore, the ^{1}(TT) formation rate in **P-PDPP-P** is significantly faster than that of other 2,2′-linked P dimers connected through conjugated bridges with comparable interchromophoric distances, highlighting the role of bridge resonance in accelerating the ^{1}(TT) formation dynamics.[35,39] Overall, the fs-TA results demonstrate that the PDPP bridge broadens the effective absorption window of the dimer system, transfers absorbed energy to the P units, and also facilitates efficient ^{1}(TT) formation.

Since the kinetics of the ^{1}(TT) state is not fully captured within the 2 ns time window of our fs-TA setup, ns-TA measurements were additionally performed to probe the subsequent dynamics after the ^{1}(TT) formation (Fig. 6). The initial TA spectrum around 3 ns could be attributed to ^{1}(TT) of **P-PDPP-P**, which is consistent with the spectral features in the late-time fs-TA results. As shown in Fig. 6B, ^{1}(TT) in **P-PDPP-P** exhibits characteristic biphasic (biexponential) dynamics similar to those observed in other P dimers.[16,34,65–67] The faster decay component ($\tau \sim 100$ ns) corresponds to the decay of the ^{m}(TT) states, including spin evolution (dephasing) from the initially prepared ^{1}(TT), and determines the yield of the final triplet excitons depending on the spin multiplicity of TT (^{1}(TT) $\rightarrow S_0$, ^{3}(TT) $\rightarrow T_1$, ^{5}(TT) $\rightarrow T_1 + T_1$), as angular momentum conservation must also be satisfied. Although TA spectroscopy is insensitive to distinguishing individual spin states of TT, it is effective in quantifying the overall triplet population.[16] The TA signal intensity after ^{m}(TT) decay is approximately half of that of the initial ^{1}(TT) signal, suggesting that the dominant decay pathway following ^{1}(TT) formation is the generation of a single T_1 exciton *via* Auger-type annihilation of ^{3}(TT). A detailed analysis of the spin evolution mechanism in **P-PDPP-P** is beyond the scope of this work. Nevertheless, ^{3}(TT) formation is

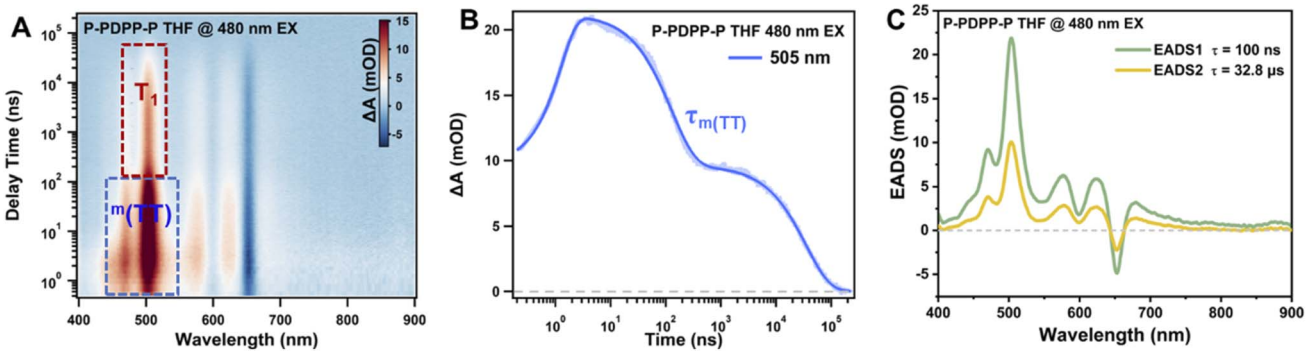

Fig. 6 ns-TA heat map of P-PDPP-P in THF at 480 nm (A) excitation, selected single wavelength kinetics traces (B), and evolution associated difference spectra (C) obtained from a global analysis.

expected to arise from anisotropic spin mixing among TT manifolds when the zero-field splitting axes of the P units are non-parallel.[7,68,69] Such a scenario is plausible, as significant torsional disorder may be present at room temperature in the solution phase. In addition, the lifetime of the final species matches that of sensitized T_1 (τ = 33 μs, Fig. 6C and S37), further supporting the assignment of the post-^{m}(TT) decay product as a single T_1 exciton. Solvent polarity does not modulate the spin evolution dynamics (Fig. S33–S36), and the relative amplitudes of the ^{m}(TT) and T_1 signals remain nearly identical across solvents, indicating comparable T_1 yields in all media. Furthermore, no qualitative differences are observed under direct P excitation, confirming that the long-lived excited-state dynamics of **P-PDPP-P** are governed exclusively by the P-centered triplet species.

Based on our experimental observations and theoretical analyses, we propose a comprehensive excited-state deactivation mechanism for **P-PDPP-P** (Fig. 7). Upon selective excitation of the PDPP unit, the excitation energy is first funneled to the P moieties *via* an ultrafast FRET process. The two adjacent P units subsequently undergo intramolecular SF to form a correlated triplet-pair intermediate, ^{1}(TT), which then undergoes spin evolution, resulting in the generation of T_1. Global analysis of the fs- and ns-TA data yields the EADSs/DADSs (Fig. 5C, F; and 6C) and corresponding time constants for the excited-state processes of **P-PDPP-P**, as summarized in Table S10. Notably, the FRET time constants in the dimer are consistently below 1 ps, indicating that the energy-transfer efficiency is near unity. Moreover, variation of the excitation wavelength does not affect the SF rate, demonstrating that the antenna-mediated excitation pathway significantly broadens the spectral window capable of triggering SF. This mechanistic picture is fully consistent with the molecular design strategy: incorporation of PDPP as a bridging antenna in **P-PDPP-P** markedly enhances light-harvesting efficiency and spectral coverage without perturbing either the SF rate or the subsequent ^{1}(TT) dissociation dynamics. In addition, solvent polarity possibly provides an effective external parameter for modulating both the energy-transfer and SF kinetics in **P-PDPP-P**.

The observed behavior here also clarifies how the present PDPP-bridged dimer differs from previously reported sensitized P dimers. In subphthalocyanine–P systems, the sensitizer primarily serves as an external light-harvesting unit that transfers excitation energy to the P dimer, after which SF proceeds within the P framework.[52] In **P-PDPP-P**, the PDPP unit plays an analogous antenna role, but it is embedded directly into the conjugated bridge. As a result, the same structural element that connects the two P units also enhances visible absorption, increases the number of effective energy-accepting pathways, and maintains a favorable transition-dipole arrangement for FRET. Importantly, the subsequent ^{1}(TT) formation dynamics are essentially identical under selective PDPP excitation and direct P excitation, demonstrating that antenna-mediated excitation broadens the absorption window without perturbing the intrinsic SF pathway of the P dimer. Thus, the present system does not simply reproduce the known antenna-assisted SF

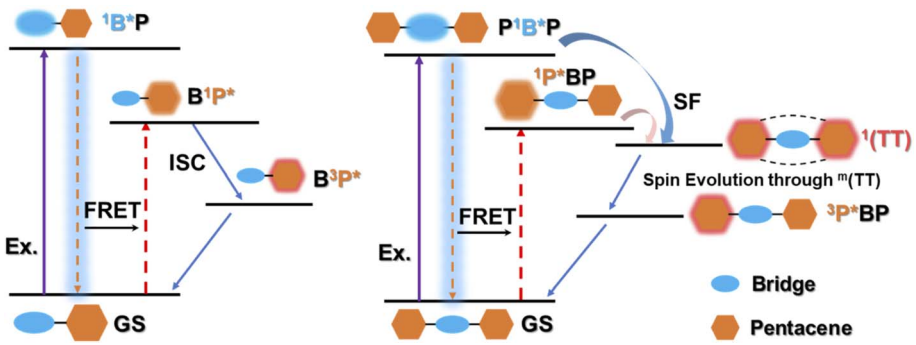

Fig. 7 Schematic diagrams for excited-state decay pathways of P-PDPP and P-PDPP-P.

concept, but extends it by showing that a compact conjugated bridge can intrinsically impose a favorable donor–acceptor dipole geometry while also providing strong absorption in the 400–550 nm region, where pentacene absorption is weak.

Conclusions

In summary, an antenna-integrated molecular design has been successfully established to address the intrinsically weak visible-light absorption of conventional P-based SF systems. By incorporating a PDPP chromophore as a functional bridging unit, the present P dimers simultaneously modulate the electronic coupling between adjacent chromophores and efficiently harvest visible light, thereby extending the spectral response of the SF system without compromising its intrinsic photophysics.

Steady-state absorption shows that the PDPP-centered molar absorption coefficient is significantly amplified as the number of flanking P units increases, leading to a markedly enhanced light-harvesting capability without altering the molecular framework. Quantum-chemical calculations further show that the moderate electronic coupling between the P and PDPP units preserves their intrinsic excited-state characteristics while simultaneously enhancing the transition dipole moment of the PDPP-centered transitions. Steady-state PL experiments reveal substantial spectral overlap between PDPP emission and P absorption, together with a high PDPP PL quantum yield, providing optimal conditions for intramolecular FRET. fs-TA measurements unambiguously confirm an ultrafast and nearly quantitative FRET process: upon selective excitation of PDPP, the excited-state energy is transferred to P on a picosecond time scale, resulting in a dramatic shortening of the PDPP excited-state lifetime from ~7 ns to ~1 ps. Quantitative FRET analysis attributes this ultrafast, near-unity process to the large orientation factor ($\kappa^2 \approx 1.15$), substantial spectral overlap integral, and high donor PLQY, resulting in a Förster radius that significantly exceeds the donor–acceptor separation. In the dimer system (**P-PDPP-P**), energy transfer from PDPP directly triggers SF, with the ^{1}(TT) formation rates identical to those obtained under direct P excitation. This finding demonstrates that the antenna-mediated excitation pathway fully preserves P's intrinsic SF dynamics while enabling broadband excitation across the entire visible solar spectrum. Notably, the transient signatures further suggest the presence of a minor but discernible direct bridge-to-dimer population pathway into the ^{1}(TT) manifold under selective PDPP excitation. Although this channel is secondary relative to FRET, it indicates that weak but non-zero orbital interactions between the bridge and the P units may provide additional electronic communication beyond purely dipole–dipole coupling. Such behavior highlights that conjugated bridges can exert a richer influence on excited-state photophysics than previously appreciated, potentially opening a new design paradigm in which bridges are engineered not only as antennas or coupling modulators, but also as active participants in multiexciton generation. Solvent polarity provides an additional handle to modulate both FRET and SF kinetics, albeit with opposite trends: increasing polarity accelerates FRET while reducing the thermodynamic driving force for SF due to stabilization and red shifting of the S_1 state of P.

Viewed in the context of previously reported P-based molecular architectures, the present results reinforce the general conclusion that efficient sensitized SF requires not only spectral overlap but also precise control over donor–acceptor transition-dipole orientation. At the same time, we extend this principle by demonstrating that a conjugated bridge can combine three functions within a single molecular element: light harvesting, directional energy funneling, and electronic communication between the SF-active chromophores. This antenna-mediated SF strategy provides an effective approach to broaden and intensify solar-light harvesting in P-based systems without altering the intrinsic structure of the SF chromophore. Although the present study centers on a P-based dimer, the underlying design principle is readily generalizable through the rational selection of bridge architectures tailored to other SF chromophores. Traditionally, bridges have been viewed primarily as structural elements that regulate the relative orientation, separation, and electronic coupling between two SF units, as mentioned above. In contrast, this work demonstrates that bridging units can play additional, active roles that positively influence SF dynamics beyond these conventional structural parameters. By elevating functional bridges from passive spacers to active light-harvesting elements, this study establishes a general molecular design framework for next-generation SF materials with enhanced solar-energy utilization.

Author contributions

W. K. conceived the project. S. P. and W. K. supervised the research. K. M. and M. K. S. synthesized the samples and performed NMR and electrochemical measurements. J. K. carried out all steady-state and time-resolved measurements, performed the quantum chemical calculations, analyzed the data, and prepared the first draft of the manuscript. S. M. conducted the preliminary fs-TA experiments. A. J. M. contributed to the mechanistic interpretation and refinement of the excited-state relaxation model. All authors discussed the results and contributed to the final version of the manuscript.

Conflicts of interest

The authors declare no competing interests.

Data availability

Data are available upon reasonable request.

Supplementary information (SI): additional details on the experimental data and quantum chemical calculations. See DOI: https://doi.org/10.1039/d6sc01678b.

Acknowledgements

W. K. acknowledges financial support from the National Research Foundation of Korea (NRF) grant funded by the Korean government (MSIT) (RS-2023-00210400 and RS-2023-00264831). W. K. also acknowledges the POSCO Science Fellowship of POSCO TJ Park Foundation. This research was

also supported by the Global Learning and Academic Research Institution for Master's, PhD Students and Postdocs (LAMP) Program of the National Research Foundation of Korea (NRF) grant funded by the Ministry of Education (RS-2024-00442483). The DFT calculations were supported by the National Institute of Supercomputing and Network (NISN)/Korea Institute of Science and Technology Information (KISTI) with needed supercomputing resources, including technical support (KSC-2025-CRE-0112). S. P. acknowledges funding support from the Department of Science and Technology (DST/ETC/CASE/RES/2023/02) and the Indian Institute of Science, Bangalore, through the REDA grant. This work was also supported by the U.S. Department of Energy, Office of Science, Condensed Phase and Interfacial Molecular Science, Chemical Sciences, Biosciences, and Geosciences Division, Early Career Research Program DE-SC0021941 (S. M. and A. J. M.).

References

1 W. Shockley and H. J. Queisser, *J. Appl. Phys.*, 1961, **32**, 510.
2 A. Rao and R. H. Friend, *Nat. Rev. Mater.*, 2017, **2**, 17063.
3 J. Xia, S. N. Sanders, W. Cheng, J. Z. Low, J. Liu, L. M. Campos and T. Sun, *Adv. Mater.*, 2017, **29**, 1601652.
4 M. C. Beard, J. M. Luther, O. E. Semonin and A. J. Nozik, *Acc. Chem. Res.*, 2013, **46**, 1252.
5 M. B. Smith and J. Michl, *Chem. Rev.*, 2010, **110**, 6891.
6 D. Casanova, *Chem. Rev.*, 2018, **118**, 7164.
7 A. J. Baldacchino, M. I. Collins, M. P. Nielsen, T. W. Schmidt, D. R. Mccamey and M. J. Y. Tayebjee, *Chem. Phys. Rev.*, 2022, **3**, 021304.
8 M. B. Smith and J. Michl, *Annu. Rev. Phys. Chem.*, 2013, **64**, 361.
9 E. Busby, J. Xia, Q. Wu, J. Z. Low, R. Song, J. R. Miller, X. Y. Zhu, L. M. Campos and M. Y. Sfeir, *Nat. Mater.*, 2015, **14**, 426.
10 M. Dvořák, S. K. K. Prasad, C. B. Dover, C. R. Forest, A. Kaleem, R. W. Macqueen, A. J. Petty II, R. Forecast, J. E. Beves, J. E. Anthony, *et al.*, *J. Am. Chem. Soc.*, 2021, **143**, 13749.
11 B. J. Walker, A. J. Musser, D. Beljonne and R. H. Friend, *Nat. Chem.*, 2013, **5**, 1019.
12 D. Thiel, H. Gotfredsen, P. M. Greißel, L. Chen, M. Krug, I. Papadopoulos, M. J. Ferguson, T. Torres, T. Clark, C. Neiss, *et al.*, *J. Am. Chem. Soc.*, 2025, **147**, 32124.
13 M. C. Hanna and A. J. Nozik, *J. Appl. Phys.*, 2006, **100**, 074510.
14 J. C. Johnson, A. J. Nozik and J. Michl, *Acc. Chem. Res.*, 2013, **46**, 1290.
15 B. S. Basel, J. Zirzlmeier, C. Hetzer, S. R. Reddy, B. T. Phelan, M. D. Krzyaniak, M. K. Volland, P. B. Coto, R. M. Young, T. Clark, *et al.*, *Chem*, 2018, **4**, 1092.
16 A. Aster, F. Zinna, C. Rumble, J. Lacour and E. Vauthey, *J. Am. Chem. Soc.*, 2021, **143**, 2361.
17 N. Monahan and X. Y. Zhu, *Annu. Rev. Phys. Chem.*, 2015, **66**, 601.
18 P. M. Zimmerman, F. Bell, D. Casanova and M. Head-Gordon, *J. Am. Chem. Soc.*, 2011, **133**, 19944.
19 S. Singh, W. J. Jones, W. Siebrand, B. P. Stoicheff and W. G. Schneider, *J. Chem. Phys.*, 1965, **42**, 330.
20 R. E. Merrifield, P. Avakian and R. P. Groff, *Chem. Phys. Lett.*, 1969, **3**, 155.
21 P. M. Zimmerman, Z. Zhang and C. B. Musgrave, *Nat. Chem.*, 2010, **2**, 648.
22 J. Zirzlmeier, D. Lehnherr, P. B. Coto, E. T. Chernick, R. Casillas, B. S. Basel, M. Thoss, R. R. Tykwinski and D. M. Guldi, *Proc. Natl. Acad. Sci. U. S. A.*, 2015, **112**, 5325.
23 S. N. Sanders, E. Kumarasamy, A. B. Pun, M. L. Steigerwald, M. Y. Sfeir and L. M. Campos, *Angew. Chem., Int. Ed.*, 2016, **55**, 3373.
24 J. C. Johnson, A. J. Nozik and J. Michl, *J. Am. Chem. Soc.*, 2010, **132**, 16302.
25 S. W. Eaton, L. E. Shoer, S. D. Karlen, S. M. Dyar, E. A. Margulies, B. S. Veldkamp, C. Ramanan, D. A. Hartzler, S. Savikhin, T. J. Marks, *et al.*, *J. Am. Chem. Soc.*, 2013, **135**, 14701.
26 A. K. Le, J. A. Bender, D. H. Arias, D. E. Cotton, J. C. Johnson and S. T. Roberts, *J. Am. Chem. Soc.*, 2018, **140**, 814.
27 F. S. Conrad-Burton, T. Liu, F. Geyer, R. Costantini, A. P. Schlaus, M. S. Spencer, J. Wang, R. H. Sánchez, B. Zhang, Q. Xu, *et al.*, *J. Am. Chem. Soc.*, 2019, **141**, 13143.
28 Y. Hong, J. Kim, W. Kim, C. Kaufmann, H. Kim, F. Würthner and D. Kim, *J. Am. Chem. Soc.*, 2020, **142**, 7845.
29 P. E. Hartnett, E. A. Margulies, C. M. Mauck, S. A. Miller, Y. Wu, Y.-L. Wu, T. J. Marks and M. R. Wasielewski, *J. Phys. Chem. B*, 2016, **120**, 1357.
30 S. Lukman, J. M. Richter, L. Yang, P. Hu, J. Wu, N. C. Greenham and A. J. Musser, *J. Am. Chem. Soc.*, 2017, **139**, 18376.
31 S. Ito, T. Nagami and M. Nakano, *J. Phys. Chem. Lett.*, 2016, **7**, 3925.
32 C. Wang and M. J. Tauber, *J. Am. Chem. Soc.*, 2010, **132**, 13988.
33 A. J. Musser, M. Maiuri, D. Brida, G. Cerullo, R. H. Friend and J. Clark, *J. Am. Chem. Soc.*, 2015, **137**, 5130.
34 S. N. Sanders, E. Kumarasamy, A. B. Pun, M. T. Trinh, B. Choi, J. Xia, E. J. Taffet, J. Z. Low, J. R. Miller, X. Roy, *et al.*, *J. Am. Chem. Soc.*, 2015, **137**, 8965.
35 M. J. Y. Tayebjee, S. N. Sanders, E. Kumarasamy, L. M. Campos, M. Y. Sfeir and D. R. Mccamey, *Nat. Phys.*, 2017, **13**, 182.
36 E. Kumarasamy, S. N. Sanders, M. J. Y. Tayebjee, A. Asadpoordarvish, T. J. H. Hele, E. G. Fuemmeler, A. B. Pun, L. M. Yablon, J. Z. Low, D. W. Paley, *et al.*, *J. Am. Chem. Soc.*, 2017, **139**, 12488.
37 J. Zirzlmeier, R. Casillas, S. R. Reddy, P. B. Coto, D. Lehnherr, E. T. Chernick, I. Papadopoulos, M. Thoss, R. R. Tykwinski and D. M. Guldi, *Nanoscale*, 2016, **8**, 10113.
38 A. B. Pun, A. Asadpoordarvish, E. Kumarasamy, M. J. Y. Tayebjee, D. Niesner, D. R. Mccamey, S. N. Sanders, L. M. Campos and M. Y. Sfeir, *Nat. Chem.*, 2019, **11**, 821.
39 K. R. Parenti, G. He, S. N. Sanders, A. B. Pun, E. Kumarasamy, M. Y. Sfeir and L. M. Campos, *J. Phys. Chem. A*, 2020, **124**, 9392.

40 K. R. Parenti, R. Chesler, G. He, P. Bhattacharyya, B. Xiao, H. Huang, D. Malinowski, J. Zhang, X. Yin, A. Shukla, *et al.*, *Nat. Chem.*, 2023, **15**, 339.
41 J. Lee, S. Eom and H. Kim, *Chem. Sci.*, 2024, **15**, 17823.
42 T. Sakuma, H. Sakai, Y. Araki, T. Mori, T. Wada, N. V. Tkachenko and T. Hasobe, *J. Phys. Chem. A*, 2016, **120**, 1867.
43 D. C. Bain, M. K. Sharma, J. Kim, S. Patil and A. J. Musser, *J. Am. Chem. Soc.*, 2025, **147**, 34989.
44 A. T. Gilligan, E. G. Miller, T. Sammakia and N. H. Damrauer, *J. Am. Chem. Soc.*, 2019, **141**, 5961.
45 J. J. Burdett, A. M. Müller, D. Gosztola and C. J. Bardeen, *J. Chem. Phys.*, 2010, **133**, 214508.
46 G. Lavarda, J. Zirzlmeier, M. Gruber, P. R. Rami, R. R. Tykwinski, T. Torres and D. M. Guldi, *Angew. Chem., Int. Ed.*, 2018, **57**, 16291.
47 D. Guzmán, I. Papadopoulos, G. Lavarda, P. R. Rami, R. R. Tykwinski, M. S. Rodríguez-Morgade, D. M. Guldi and T. Torres, *Angew. Chem., Int. Ed.*, 2021, **60**, 1474.
48 J. Zirzlmeier, G. Lavarda, H. Gotfredsen, I. Papadopoulos, L. Chen, T. Clark, R. R. Tykwinski, T. Torres and D. M. Guldi, *Nanoscale*, 2020, **12**, 23061.
49 P. M. Greißel, D. Thiel, H. Gotfredsen, L. Chen, M. Krug, I. Papadopoulos, M. Miskolzie, T. Torres, T. Clark, M. Brøndsted Nielsen, *et al.*, *Angew. Chem., Int. Ed.*, 2024, **63**, e202315064.
50 T. Mirkovic, E. E. Ostroumov, J. M. Anna, R. Van Grondelle, Govindjee and G. D. Scholes, *Chem. Rev.*, 2017, **117**, 249.
51 D. Guzmán, I. Papadopoulos, G. Lavarda, P. R. Rami, R. R. Tykwinski, M. S. Rodríguez-Morgade, D. M. Guldi and T. Torres, *Angew. Chem., Int. Ed.*, 2021, **60**, 1474.
52 H. Gotfredsen, D. Thiel, P. M. Greißel, L. Chen, M. Krug, I. Papadopoulos, M. J. Ferguson, M. B. Nielsen, T. Torres, T. Clark, *et al.*, *J. Am. Chem. Soc.*, 2023, **145**, 9548.
53 A.-S. Wollny, G. Lavarda, I. Papadopoulos, I. López-Duarte, H. Gotfredsen, Y. Hou, R. R. Tykwinski, T. Torres and D. M. Guldi, *Adv. Opt. Mater.*, 2023, **11**, 2300500.
54 D.-P. Medina, I. Papadopoulos, G. Lavarda, H. Gotfredsen, P. R. Rami, R. R. Tykwinski, M. S. Rodríguez-Morgade, D. M. Guldi and T. Torres, *Nanoscale*, 2019, **11**, 22286.
55 S. Celik, Y. Ergun and S. Alp, *J. Fluoresc.*, 2009, **19**, 829.
56 W. Kim, N. A. Panjwani, K. C. Krishnapriya, K. Majumder, J. Dasgupta, R. Bittl, S. Patil and A. J. Musser, *Cell Rep. Phys. Sci.*, 2024, **5**, 102045.
57 K. C. Krishnapriya, P. Roy, B. Puttaraju, U. Salzner, A. J. Musser, M. Jain, J. Dasgupta and S. Patil, *Nat. Commun.*, 2019, **10**, 33.
58 N. E. Geacintov, J. Burgos, M. Pope and C. Strom, *Chem. Phys. Lett.*, 1971, **11**, 504.
59 J. Lee, J. Kim, J. Kim and W. Kim, *Synth. Met.*, 2026, **317**, 118078.
60 T. Lu and F. Chen, *J. Comput. Chem.*, 2012, **33**, 580.
61 T. Lu, *J. Chem. Phys.*, 2024, **161**, 082503.
62 İ. Sıdır and Y. G. Sıdır, *J. Mol. Liq.*, 2016, **221**, 972.
63 H. Zhu, M. Li, J. Hu, X. Wang, J. Jie, Q. Guo, C. Chen and A. Xia, *Sci. Rep.*, 2016, **6**, 24313.
64 A. Olaya-Castro and G. D. Scholes, *Int. Rev. Phys. Chem.*, 2011, **30**, 49.
65 B. S. Basel, J. Zirzlmeier, C. Hetzer, B. T. Phelan, M. D. Krzyaniak, S. R. Reddy, P. B. Coto, N. E. Horwitz, R. M. Young, F. J. White, *et al.*, *Nat. Commun.*, 2017, **8**, 15171.
66 G. He, K. R. Parenti, J. K. Bindra, J. Niklas, S. J. Baker, B. Salcido-Santacruz, I. D. Dergachev, C. E. Avalos, O. G. Poluektov, S. Mazumdar, *et al.*, *J. Am. Chem. Soc.*, 2026, **148**, 8146.
67 K. Majumder, S. Mukherjee, J. Park, W. Kim, A. J. Musser and S. Patil, *Angew. Chem., Int. Ed.*, 2024, **63**, e202408615.
68 T. S. C. Macdonald, M. J. Y. Tayebjee, M. I. Collins, E. Kumarasamy, S. N. Sanders, M. Y. Sfeir, L. M. Campos and D. R. Mccamey, *J. Am. Chem. Soc.*, 2023, **145**, 15275.
69 T. Hasobe, S. Nakamura, N. V. Tkachenko and Y. Kobori, *ACS Energy Lett.*, 2022, **7**, 390.